

Crossed-beam reaction of carbon atoms with hydrocarbon molecules. IV. Chemical dynamics of methylpropargyl radical formation, C_4H_5 , from reaction of $C(^3P_j)$ with propylene, C_3H_6 (X^1A')

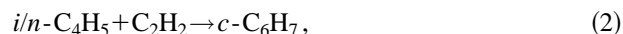
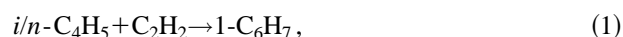
R. I. Kaiser, D. Stranges,^{a)} H. M. Bevsek, Y. T. Lee,^{b)} and A. G. Suits
Department of Chemistry, University of California, Berkeley, California 94720 and Chemical Sciences Division, Berkeley National Laboratory, Berkeley, California 94720

(Received 3 October 1996; accepted 19 December 1996)

The reaction between ground state carbon atoms and propylene, C_3H_6 , was studied at average collision energies of 23.3 and 45.0 kJ mol^{-1} using the crossed molecular beam technique. Product angular distributions and time-of-flight spectra of C_4H_5 at $m/e=53$ were recorded. Forward-convolution fitting of the data yields a maximum energy release as well as angular distributions consistent with the formation of methylpropargyl radicals. Reaction dynamics inferred from the experimental results suggest that the reaction proceeds on the lowest 3A surface via an initial addition of the carbon atom to the π -orbital to form a triplet methylcyclopropylidene collision complex followed by ring opening to triplet 1,2-butadiene. Within 0.3–0.6 ps, 1,2-butadiene decomposes through carbon–hydrogen bond rupture to atomic hydrogen and methylpropargyl radicals. The explicit identification of C_4H_5 under single collision conditions represents a further example of a carbon–hydrogen exchange in reactions of ground state carbon with unsaturated hydrocarbons. This versatile machine represents an alternative pathway to build up unsaturated hydrocarbon chains in combustion processes, chemical vapor deposition, and in the interstellar medium. © 1997 American Institute of Physics. [S0021-9606(97)01812-6]

I. INTRODUCTION

Sophisticated combustion models of oxidative hydrocarbon flames postulate that synthesis of polycyclic aromatic hydrocarbons (PAHs) and formation of soot particles are strongly related and are initiated by stepwise reaction of smaller hydrocarbon radicals to cyclohexadienyl [reactions (1)–(2)] or benzene [reaction (3)]:^{1,2}



However, the explicit mechanism to form distinct C_4H_5 isomers is still elusive. Wang and Frenklach³ as well as Millar and Melius² assume reaction of vinyl radicals with acetylene via a long-lived, rovibrationally excited (*) C_4H_5 adduct which fragments either to C_4H_4 or is stabilized in a third body collision (M):



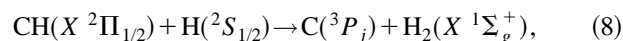
Weissman *et al.* pointed out reaction (4) should lead exclusively to $n-C_4H_5$,⁴ but isomerization might transform iso to normal isomers via reaction (7),² Fig. 1:



^{a)}Present address: Dipartimento Chimica, Universita La Sapienza, Piazzale A. Moro 5, 00185 Rome, Italy.

^{b)}Present address: Academia Sinica, Nankang, Taipei, 11529, Taiwan.

The spectroscopic identification of CH radicals, even in oxidative hydrocarbon flames, opens an alternative pathway to C_4H_5 isomers,⁵ since atomic hydrogen reacts in these media with CH to atomic carbon and molecular hydrogen [reaction (8)] followed by a likely addition of $C(^3P_j)$ to the carbon–carbon double bond of propylene to form an internally excited (*) triplet C_4H_6 isomer [reaction (9)]. This collision complex can decompose via hydrogen emission to C_4H_5 :



Besides their latent combustion relevance, propylene and C_4H_5 isomers are expected to contribute to interstellar chemistry. Although neither C_3H_6 nor C_4H_5 have been identified in the interstellar medium (ISM) explicitly, the extraterrestrial propylene existence seems reasonable since unsubstituted C_2H_4 was detected in the circumstellar envelope of the evolved carbon star IRC+10216 and the two lowest alkynes acetylene (C_2H_2) and methylacetylene (CH_3CCH) are ubiquitous in the ISM.⁶ Beyond its interstellar relevance, Voyager data depict propylene in Titan's and in the upper Neptunian atmosphere.^{7–10} Recent MeV and keV ion induced collision cascade simulations in hydrocarbon ices¹¹ as well as planetary atmospheres¹² show a production rate of, e.g., 70 suprathreshold knock-on carbon atoms per impinging 12 keV carbon atom originating from the solar radiation field. Since the knock-on atoms are born with kinetic energies up to 1 keV, they cannot form stable chemical bonds and survive reducing planetary atmospheres to kinetic energies less

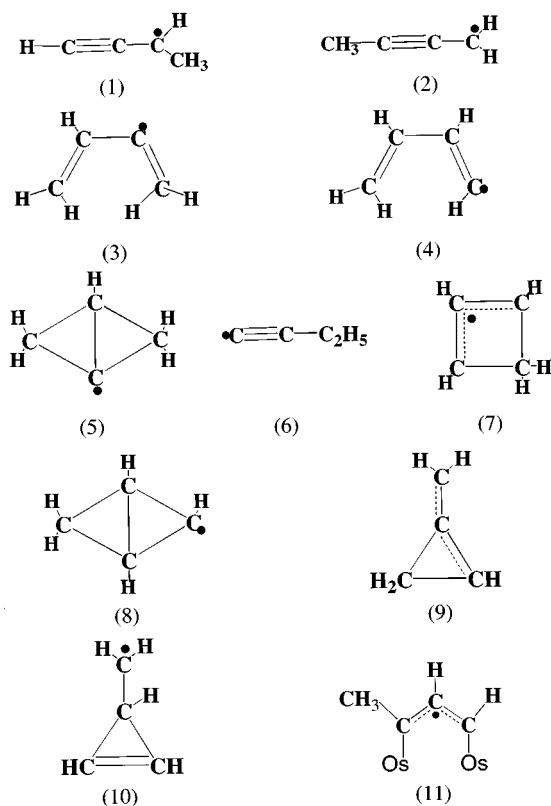


FIG. 1. Structures of distinct C_4H_5 isomers. Enthalpies of formations are given in the text.

than ca. 10 eV. At the endpoints of their trajectories, atomic carbon can react with unsaturated hydrocarbons such as propylene via reaction (9).

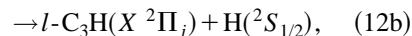
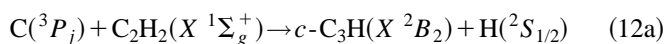
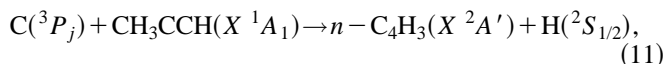
Despite the astrochemical and combustion potential, the characterization of the doublet C_4H_5 potential energy surface (PES) has been neglected. Low and high pressure pyrolysis experiments indicate that 1- or 3-methylpropargyl (1)/(2) hold the global minimum [$\Delta_f H_0^0(1) = 295 \pm 10$ kJ mol $^{-1}$; $\Delta_f H_0^0(2) = 294 \pm 3$ kJ mol $^{-1}$],^{13–16} Fig. 1. Two less stable radicals, 1,3-butadienyl-2 and 1,3-butadienyl-1 follow with $\Delta_f H_0^0(3) = 344 \pm 10$ kJ mol $^{-1}$ and $\Delta_f H_0^0(4) = 357 \pm 10$ kJ mol $^{-1}$, respectively.^{3,16,17} Additionally, the enthalpy of formation of the bicyclo[1.1.0]-butyl, (5), as well as the butynyl-1 radical, (6), were determined to be 427 ± 33 and 485 ± 17 kJ mol $^{-1}$.¹⁸ Due to their high reactivity, strained C_4H_5 isomers (7)–(10) could only be identified in solid matrices at 77 K via ESR spectroscopy after irradiating distinct hydrocarbon precursors with Co⁶⁰ γ -rays, but thermodynamical data are missing.^{19–24} Finally, a methylallyl isomer which even resisted matrix trapping was stabilized by metal atoms as a μ_3 -diosmiumate complex (11).²⁵

The work reported here is part of an ongoing project to elucidate the potential energy surfaces and chemical reaction dynamics of carbon atoms in their $C(^3P_j)$ electronic ground state with unsaturated hydrocarbons under single collision conditions. Papers I–III disclosed precise information on the formation of propargyl [reaction (10)],²⁶ α -ethynylvinyl [re-

TABLE I. Experimental beam conditions and 1σ errors: most probable velocity v_0 , speed ratio S , most probable relative collision energy with the propylene molecules, E_{coll} , center-of-mass angle, θ_{CM} , and composition of the carbon beam?: no information available.

Beam	v_0 , m s $^{-1}$	S	E_{coll} , kJ mol $^{-1}$	θ_{CM}	$C_1:C_2:C_3$
$C(^3P_j)/\text{Ne}$	2090 ± 50	5.2 ± 0.3	23.3 ± 1.0	52.7 ± 0.9	1:0.5:1.5
$C(^3P_j)/\text{He}$	3000 ± 75	2.6 ± 0.2	45.0 ± 4.0	42.5 ± 1.5	?
C_3H_6	783 ± 12	8.3 ± 0.2

action (11)],²⁷ and tricarbon-hydrides [reactions (12a/b)]:^{28–30}



and initially formed triplet collision complexes. Here, we investigate the detailed chemical dynamics of $C(^3P_j)$ reactive encounters with propylene at nominal collision energies of 23.3 kJ mol $^{-1}$ and 45.0 kJ mol $^{-1}$ to tetracarbon hydrides C_4H_x ($x=0-5$) of potential interstellar and combustion chemistry relevance.

II. EXPERIMENTAL SETUP

Reactive scattering experiments are performed in a universal crossed molecular beam apparatus.³¹ Briefly, a pulsed supersonic carbon beam was generated via laser ablation of graphite at 266 nm from a quadrupled Nd:YAG laser.³² The present design of our carbon source differs slightly from Ref. 32. Both micro switches that triggered the polarity switch of the stepper motor were replaced by a resistance based position indicator interfaced to the rotating graphite rod. This improved version prevents shorting of the micro switch circuit as graphite condenses during the operation. The 30 Hz, 35–40 mJ laser output is focused onto a rotating carbon rod, and ablated carbon atoms are seeded into neon (99.999%, Bay Area Gas) or helium (99.999%, Bay Area Gas) released by a Proch-Trickl pulsed valve. A four slot chopper wheel is mounted after the ablation zone and selects a 9.0 μs segment of the seeded carbon beam. Table I compiles the experimental beam conditions. The pulsed carbon beam and a continuous propylene (99.995%, Matheson) beam with 558 ± 11 Torr backing pressure pass through skimmers and cross at 90° in the interaction region of the scattering chamber at relative collision energies of 23.3 and 45.0 kJ mol $^{-1}$. Reactively scattered products were detected in the plane of the beams using a rotatable detector with a Brink-type electron-impact ionizer,³³ quadrupole mass filter, and a Daly ion detector³⁴ at different laboratory angles between 5.0° and 60.0° with respect to the carbon beam. Velocity distributions of the products were recorded using the time-of-flight (TOF)

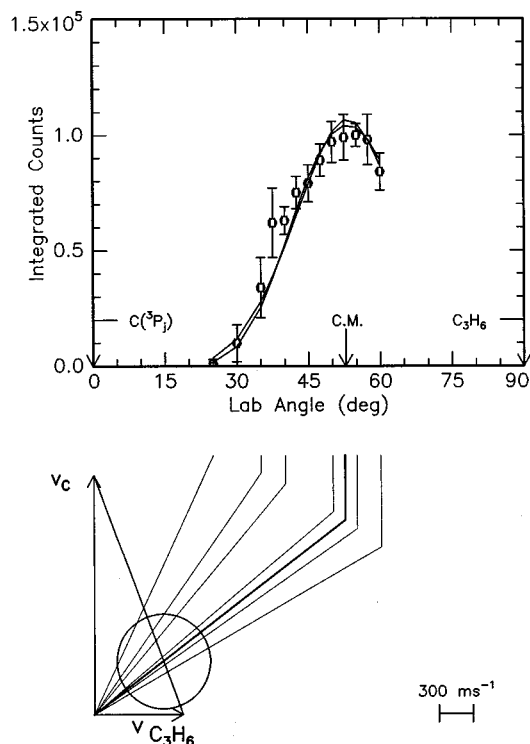


FIG. 2. Lower: Newton diagram for the reaction $C(^3P_j) + C_3H_6(X^1A')$ at a collision energy of 23.3 kJ mol^{-1} . The circle stands for the maximum center-of-mass recoil velocity assuming no internal excitation. Upper: Laboratory angular distribution of product channel at $m/e=53$. Circles and 1σ error bars indicate experimental data, the solid lines the calculated distributions for the upper and lower carbon beam velocity. CM designates the center-of-mass angle. The solid lines point to distinct laboratory angles whose TOFs are shown in Fig. 4.

technique. Reference angles were chosen at 55° and 40° to calibrate fluctuating carbon beam intensities and mass dial settings at the quadrupole controller.

For the physical interpretation of the scattering data it is necessary to transform the laboratory data into the center-of-mass (CM) reference frame. A forward-convolution routine is used to fit the TOF spectra and the product angular distribution in the laboratory frame (LAB distribution).^{35,36} This procedure initially guesses the angular flux distribution $T(\theta)$ and the translational energy flux distribution $P(E_T)$ in the center-of-mass system (CM). TOF spectra and the LAB distribution are calculated from $T(\theta)$ and $P(E_T)$ and refined iteratively until a reasonable fit is achieved. The ultimate outcome is the generation of a velocity flux contour map showing the intensity as a function of angle and velocity in the CM frame. This map serves as an image of the reaction and contains all information of the scattering process.

III. RESULTS

A. Reactive scattering signal

Reactive scattering signal was only detected at $m/e=53$, i.e., C_4H_5 , cf. Figs. 2–5. TOF spectra of lower m/e values between 52 and 48 were monitored and reveal identical patterns. Therefore, this signal originates in cracking of the

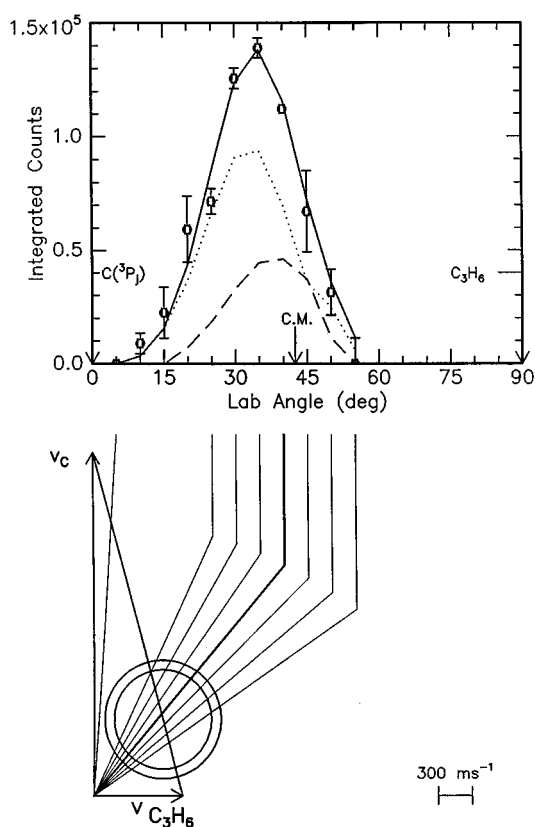


FIG. 3. Lower: Newton diagram for the reaction $C(^3P_j) + C_3H_6(X^1A')$ at a collision energy of 45.0 kJ mol^{-1} . The circle stands for the maximum center-of-mass recoil velocity assuming no internal excitation. Upper: Laboratory angular distribution of product channel at $m/e=53$. Circles and 1σ error bars indicate experimental data, the solid lines the calculated distributions for the upper and lower carbon beam velocity. Dotted lines show the contribution from $C(^1D_2)$, dashed lines from $C(^3P_j)$. CM designates the center-of-mass angle. The solid lines point to distinct laboratory angles whose TOFs are shown in Fig. 5.

C_4H_5 parent in the ionizer, and exothermic channels 7–9 are absent within detection limits (Table II). Additionally, no radiative association to C_4H_6 ($m/e=54$) or higher masses were observed. Endothermic channels 10 and 11 could not be opened at relative collision energies up to 45.0 kJ mol^{-1} employed in our experiments.

B. LAB distribution and TOF spectra

Figures 2 and 3 show the most probable Newton diagrams of the reaction $C(^3P_j) + C_3H_6(X^1A')$ together with the laboratory angular distributions (LAB) of the C_4H_5 product at collision energies of 23.3 and 45.0 kJ mol^{-1} , respectively. At higher energy, the carbon beam contains contributions from electronically excited $C(^1D_2)$ state, whose reaction dynamics with acetylene, ethylene, methylacetylene, and propylene are subject of a forthcoming article.³⁷ As the collision energy E_{coll} rises, the maximum of the LAB distribution shifts from the center-of-mass angle $\theta_{\text{CM}}=52.7\pm 0.9^\circ$ ($E_{\text{coll}}=23.3 \text{ kJ mol}^{-1}$) to a slightly forward position of about 40.0° versus $\theta_{\text{CM}}=42.5\pm 1.0^\circ$ [$E_{\text{coll}}=45.0 \text{ kJ mol}^{-1}$; $C(^3P_j)$ contribution only]. These data suggest a reduced lifetime of

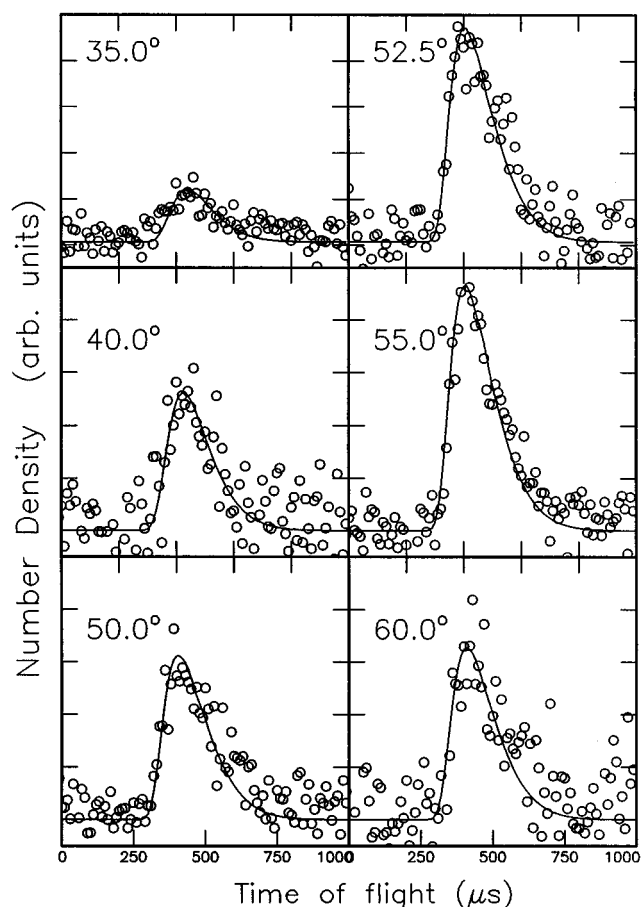


FIG. 4. Time-of-flight data at $m/e=53$ for laboratory angles 35.0 , 40.0 , 50.0 , 52.5 , 55.0 , and 60.0° at a collision energy of 23.3 kJ mol^{-1} . Open circles represent experimental data, the solid line the fit. TOF spectra have been normalized to the relative intensity at each angle.

the decomposing C_4H_6 complex with rising collision energy. Further, both LAB distributions are very broad and spread about 50° in the scattering plane. This finding proposes a large energy release into translational degrees of freedom of the C_4H_5 and H products as well as a center-of-mass translational energy distribution peaking away from zero. A comparison of the scattering range at lower energy with the limit circle of the methylpropargyl isomers correlates with the signal cut off at 25° and suggests a significant contribution of these isomers to the reactive scattering signal.

C. Center-of-mass translational energy distributions, $P(E_T)$

The translational energy distributions $P(E_T)$ and the angular distributions $T(\theta)$ in the center-of-mass frame are presented in Figs. 6 and 7. Best fits of TOF spectra and LAB distributions were achieved with $P(E_T)$ s extending to $E_{\text{max}}=200\text{--}225 \text{ kJ mol}^{-1}$ and $260\text{--}280 \text{ kJ mol}^{-1}$, respectively. These energy cutoffs can be utilized to identify the product isomer if their energetics are well separated. At lower collision energy, E_{max} suggests formation of methylpropargyl and/or 1,3-butadienyl radicals within the error limits cf. Fig. 1 and Table III. At $E_{\text{coll}}=45.0 \text{ kJ mol}^{-1}$, the maxi-

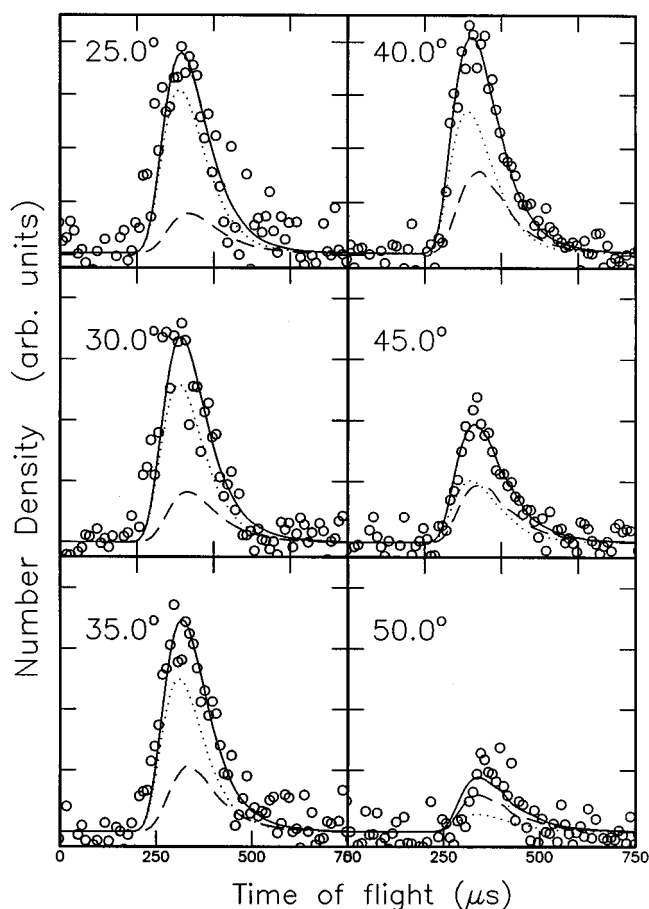


FIG. 5. Time-of-flight data at $m/e=53$ for laboratory angles 25.0 , 30.0 , 35.0 , 40.0 , 45.0 , and 50.0° at a collision energy of 45.0 kJ mol^{-1} . Open circles represent experimental data, the solid line the fit. Dotted lines show the contribution from $\text{C}(^1D_2)$, dashed lines from $\text{C}(^3P)$. TOF spectra have been normalized to the relative intensity at each angle.

um translational energy is consistent with the formation of methylpropargyl isomers. Further, the most probable translational energy yields an order-of-magnitude of the barrier height in the exit channel. Both $P(E_T)$ s show a broad plateau

TABLE II. Thermochemistry of the reaction $\text{C}(^3P_j) + \text{C}_3\text{H}_6(X^1A')$ to C_4H_x products. Channels were calculated for the most stable isomer, i.e., C_4H_4 (butatriene; channel 7), C_4H_3 (α -ethynylvinyl; channel 8), C_4H_2 (diacetylene; channel 9), C_4H (tetracarbonhydride; channel 10), and C_4 (tetracarbon; channel 11).

#	Exit channel	Free reaction enthalpy at 0 K, $\Delta_R H(0 \text{ K})$, kJ mol^{-1}
1	$\text{HCCCHCH}_3(X^2A'') + \text{H}(^2S_{1/2})$	-220 ± 10
2	$\text{CH}_3\text{CCCH}_2(X^2B_1) + \text{H}(^2S_{1/2})$	-221 ± 3
3	$\text{H}_2\text{CHCCCH}_2(X^2A') + \text{H}(^2S_{1/2})$	-171 ± 10
4	$\text{H}_2\text{CHCHCHC}(X^2A') + \text{H}(^2S_{1/2})$	-158 ± 10
5	$c\text{-C}_4\text{H}_5(X^2A') + \text{H}(^2S_{1/2})$	-88 ± 33
6	$\text{C}_2\text{H}_5\text{CC}(X^2A') + \text{H}(^2S_{1/2})$	-30 ± 17
7	$\text{C}_4\text{H}_4(X^1A_g) + \text{H}_2(X^1\Sigma_g^+)$	-442 ± 2
8	$\text{C}_4\text{H}_3(X^2A') + \text{H}_2(X^1\Sigma_g^+) + \text{H}(^2S_{1/2})$	-5 ± 35
9	$\text{C}_4\text{H}_2(X^1\Sigma_g^+) + 2\text{H}_2(X^1\Sigma_g^+)$	-279 ± 12
10	$\text{C}_4\text{H}(X^2\Sigma^+) + 2\text{H}_2(X^1\Sigma_g^+) + \text{H}(^2S_{1/2})$	$+243 \pm 5$
11	$\text{C}_4(X^3\Sigma_g^-) + 3\text{H}_2(X^1\Sigma_g^+)$	$+232 \pm 5$

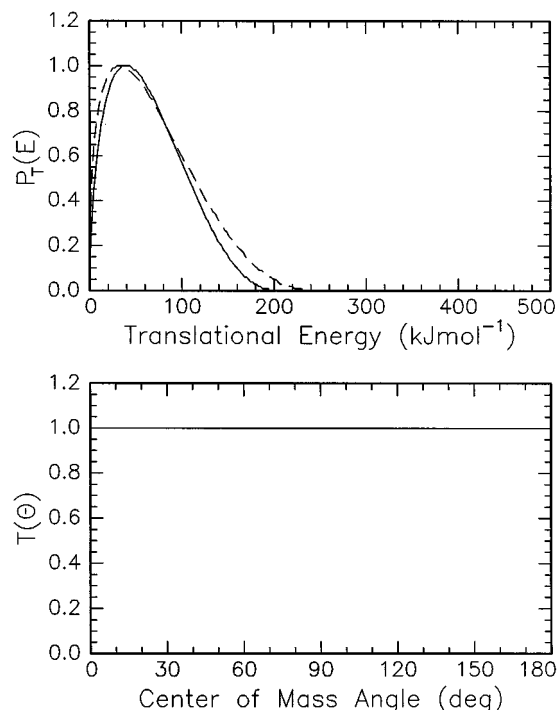


FIG. 6. Lower: Center-of-mass angular flux distribution for the reaction $C(^3P_j)+C_3H_6(X^1A')$ at a collision energy of 23.3 kJ mol^{-1} . Upper: Center-of-mass translational energy flux distribution for the reaction $C(^3P_j)+C_3H_6(X^1A')$ at a collision energy of 23.3 kJ mol^{-1} . Dashed and solid lines limit the range of acceptable fits within 1σ error bars.

between 15 and 60 kJ mol^{-1} , indicating a tight exit transition state as well as a significant electron density change from the C_4H_6 complex to the products. A potential energy barrier in the exit channel is further indicated by the large fraction of total available energy released into translational motion of the products, i.e., $31 \pm 4\%$ and $34 \pm 3\%$ at 23.3 and 45.0 kJ mol^{-1} , respectively.

D. Center-of-mass angular distributions, $T(\theta)$

As the collision energy rises, the shape of both $T(\theta)$ s changes significantly. At lower collision energy, the $T(\theta)$ is isotropic and symmetric around $\pi/2$ suggesting that the decomposing C_4H_6 complex has a lifetime longer than its rotational period or that the exit transition state is symmetric.^{26,38,39} With rising collision energy, the center-of-mass angular distribution peaks forward with respect to the carbon beam and shows an intensity ratio at the poles of $I(0^\circ)/I(180^\circ) = 6 \pm 3$. This trend is reflected in the center-of-mass flux contour maps $I(\theta) \sim T(\theta) * P(E_T)$ as well, cf. Figs. 8 and 9. Our results strongly indicate a reduced lifetime of the C_4H_6 intermediate and suggest an osculating complex: a complex formation takes place, but the well depth along the reaction coordinate is too shallow to allow multiple rotations, and the complex decomposes with a random lifetime distribution before one full rotation elapses. In Sec. IV, we identify this complex and estimate its lifetime. Further, the

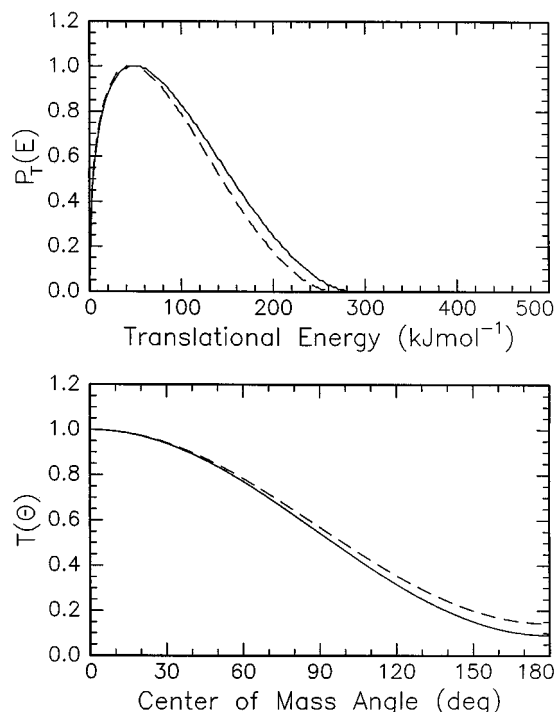


FIG. 7. Lower: Center-of-mass angular flux distribution for the reaction $C(^3P_j)+C_3H_6(X^1A')$ at a collision energy of 45.0 kJ mol^{-1} . Upper: Center-of-mass translational energy flux distribution for the reaction $C(^3P_j)+C_3H_6(X^1A')$ at a collision energy of 45.0 kJ mol^{-1} . Dashed and solid lines limit the range of acceptable fits within 1σ error bars.

carbon atom and the leaving hydrogen atom must be located forward peaking at higher collision energy requires that the on opposite sites of the rotation axis of the fragmenting complex.

The lack of polarization of the angular distribution at $E_{\text{coll}} = 23.3 \text{ kJ mol}^{-1}$ is the result of a poor correlation between the initial and final angular momentum vectors, \mathbf{L} and \mathbf{L}' , respectively.^{26,38,39} Calculating the maximum impact parameter b_{max} and the maximum orbital angular momentum L_{max} within the orbiting limit and approximating the Lennard-Jones coefficient C_6 according to Hirschfelder *et al.*⁴⁰ with the ionization potentials of $C(^3P_j)$ and propylene of 11.76 eV , and 10.36 eV , respectively, and polarizabilities of $C(^3P_j)$ and propylene, $1.76 \times 10^{-30} \text{ m}^3$ and $6.24 \times 10^{-30} \text{ m}^3$,⁴¹ b_{max} yields $b_{\text{max}}(23.3 \text{ kJ mol}^{-1}) = 3.7 \text{ \AA}$, $b_{\text{max}}(45.0 \text{ kJ mol}^{-1}) = 3.3 \text{ \AA}$, $L_{\text{max}}(23.3 \text{ kJ mol}^{-1}) = 122\hbar$ and $L_{\text{max}}(45.0 \text{ kJ mol}^{-1}) = 151\hbar$. If we compare this order-of-magnitude calculation with the final orbital angular momentum \mathbf{L}' as derived from acceptable exit impact parameters,

TABLE III. Lifetime t in ps of triplet *cis* and *trans* 1,2-butadiene calculated for rotations about the A, B, and C axis at collision energy of 45.0 kJ mol^{-1} . Errors are 28%. Units of principal moments of inertia are given in amu \AA^2 .

Isomer	I_A	I_B	I_C	$t(A)$	$t(B)$	$t(C)$
<i>cis</i>	14.5949	79.3413	93.9362	0.05	0.3	0.35
<i>trans</i>	6.7936	99.8642	106.6578	0.02	0.4	0.55

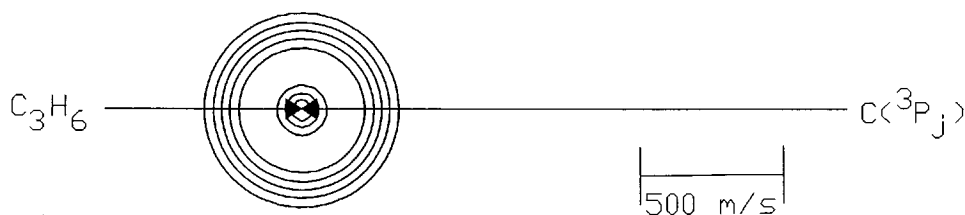


FIG. 8. Contour flux map distribution for the reaction $C(^3P_j) + C_3H_6(X^1A')$ at a collision energy of 23.3 kJ mol^{-1} .

cf. Sec. V and Fig. 10, we find $L < 0.2L'$. Therefore, most of the initial orbital angular momentum channels into rotational excitation of the C_4H_5 products to yield a flat angular distribution at lower collision energy. This result is the direct consequence of large impact parameters leading to C_4H_6 complex formation and the inability of the hydrogen atom to carry away a significant amount of orbital angular momentum.

V. DISCUSSION

In this section, we investigate energetically feasible reaction pathways on the triplet C_4H_6 PES via insertion of the electrophile carbon atoms into the C–H– and C–C bonds of propylene as well as addition to the π -molecular orbital. The experimental CM angular and translational energy distributions are then compared to what is expected based on these postulated channels. Since no C_4H_6 intermediate fulfills requirements for intersystem crossing,⁴² the discussion is restricted to the triplet surface. We establish that $C(^3P_j)$ interacts with the π -electron density to form methylcyclopropylidene followed by ring opening to triplet 1,2-butadiene. This complex decomposes to a methylpropargyl radical and atomic hydrogen.

A. Insertion pathway

As outlined in the previous section, large impact parameters up to $b = 3.7 \text{ \AA}$ contribute predominantly to the reactive scattering signal. If we compare this dimension with impact parameters to $C(^3P_j)$ insertion into the olefinic C–H– and C–C as well as aliphatic C–H bonds of propylene, we estimate an upper limit of only 1.4, 0.9, and 1.5 \AA . Therefore, any insertion can be very likely ruled out. This conclusion correlates strongly with related systems studied recently in our group. Here, no $C(^3P_j)$ insertion into an aliphatic C–H bonds of CH_4 (Ref. 43) and CH_3 group in methylacetylene was found.²⁷ Further, the chemical dynamics of the $C(^3P_j)/C_2H_4$ system are solely determined by the interaction

of the carbon atom with the π -electron density, and no insertion into the olefinic C–H bond was verified.²⁶ Finally, the hydrogen atoms screen the aliphatic C–C bond in propylene from insertion: even hot atom tracer experiments with $^{11}C(^3P_j)$ show no insertion into C–C single bonds.⁴⁴

B. Addition pathway

The reaction dynamics of the title reaction are controlled by addition of the carbon atom to the olefinic carbon–carbon bond of the propylene molecule under C_1 symmetry to form methylcyclopropylidene, cf. Fig. 10. This pathway does not require solely an on-axis approach of the $C(^3P_j)$ p -orbital toward the π -molecular orbital, but permits trajectories in which p -orbitals are skewed with respect to the propylene plane. This opens larger impact parameters than typical C_3H_6 bond dimensions compared to the large b dominated opacity function as discussed in Sec. IV D. Initially, $C(^3P_j)$ attacks either the α -carbon atom, i.e., the neighboring carbon atom to the CH_3 group, or the β -C atom holding the CH_2 unit prior to ring closure. If we apply the framework of regioselectivity of electrophilic attacks to substituted olefines,⁴⁵ we discriminate between these two options. This concept predicts the electrophilic attack is directed preferentially to the carbon center retaining the maximum spin density of the first excited $^3\pi\pi^*$ state. Since *ab initio* calculations show that the β -C atom holds a spin density of 1.232 versus 1.216 at the α -C, $C(^3P_j)$ should attack preferentially the β -position. In addition, the methyl group reduces the cone of acceptance on the α -C atom as well and directs the approach even more to the β -position. The pathway to methylcyclopropylidene correlates with previous $^{11}C(^3P_j)$ bulk experiments, in which cyclopropylidene intermediates were trapped as spiranes.⁴⁴

The fate of the methylcyclopropylidene is governed either by hydrogen migration to methylcyclopropane isomers or conrotatory ring opening to *cis/trans* 1,2-butadiene. Any H rearrangement, however, can be excluded: the methylcyclopropane isomers would undergo a subsequent C–H bond

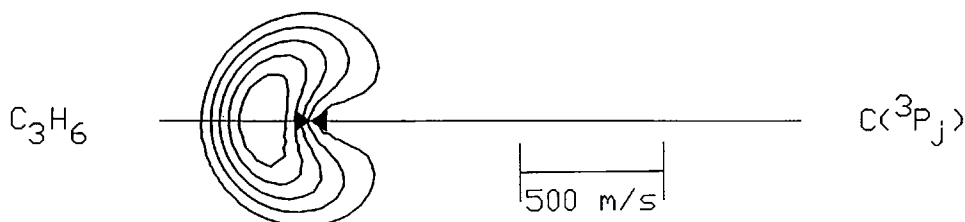


FIG. 9. Contour flux map distribution for the reaction $C(^3P_j) + C_3H_6(X^1A')$ at a collision energy of 45.0 kJ mol^{-1} .

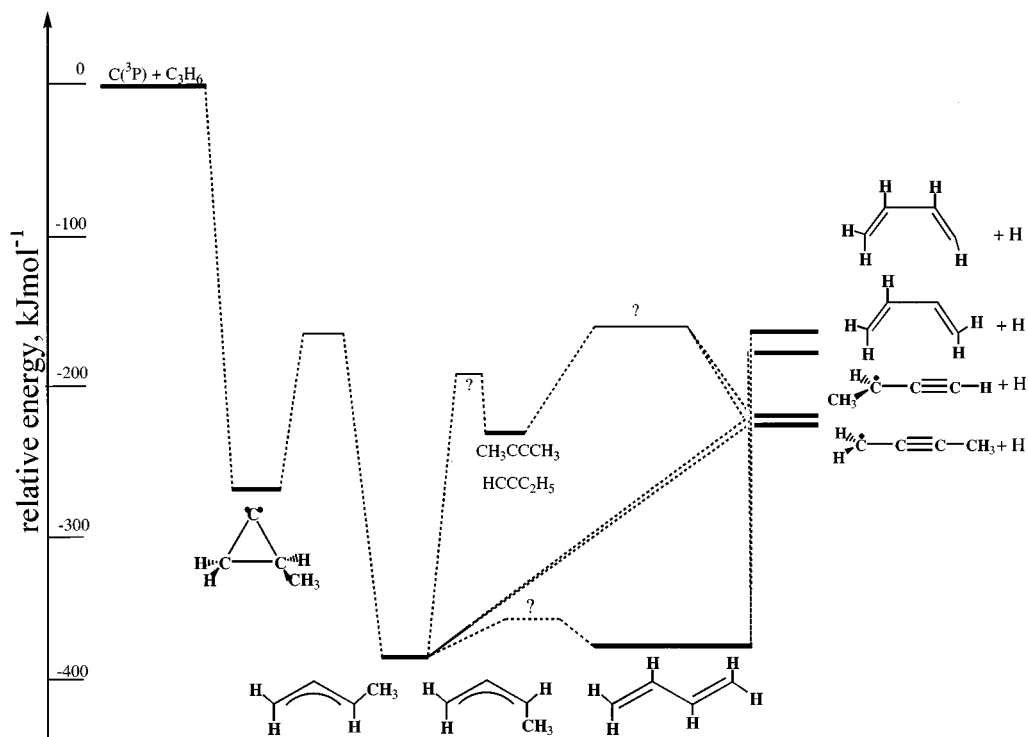


FIG. 10. Schematic representation of the lowest energy pathways on the triplet C_4H_6 PES and structures of potentially involved collision complexes. ? : no information available (Refs. 13–25,41).

rupture to a carbontricyclic. Even the energetically most favorable isomer, methylcyclopropyl, is at least ca. 100 kJ mol^{-1} less stable than methylpropargyl. Therefore, the reaction exothermicity of only 130 kJ mol^{-1} cannot account for the high energy cutoffs of both translational energy distributions. Therefore, the conrotatory ring opening to 1,2-butadiene remains the only open path. This ring opening can proceed via a clockwise–clockwise (I) as well as counterclockwise–counterclockwise (II) rotation of the CH_2 and $\text{CH}(\text{CH}_3)$ units, cf. Fig. 11. Pathway I leads solely to *cis* 1,2-butadiene, whereas II forms only the *trans* isomer. Since an enhanced repulsive potential between the CH_3 group and the hydrogen atom is expected in pathway I versus two in-

teracting H atoms (pathway II), the transition state in I is anticipated to be energetically less favorable. Hence, *trans*-1,2-butadiene should be formed preferentially. Since no *ab initio* frequencies of the transition states are available, we cannot quantify the relative fraction of the clockwise versus counterclockwise direction.

1,2-butadiene either undergoes hydrogen rearrangement to 1,3-butadiene, dimethylacetylene, or ethyl-acetylene or fragments via C–H bond rupture to methylpropargyl. Since these H migrations are symmetry allowed, reaction to 1,3-butadiene is expected to involve a barrier much less than at least 140 kJ mol^{-1} from 1,2-butadiene to acetylene derivatives. However, both acetylene derivatives can likely be ex-

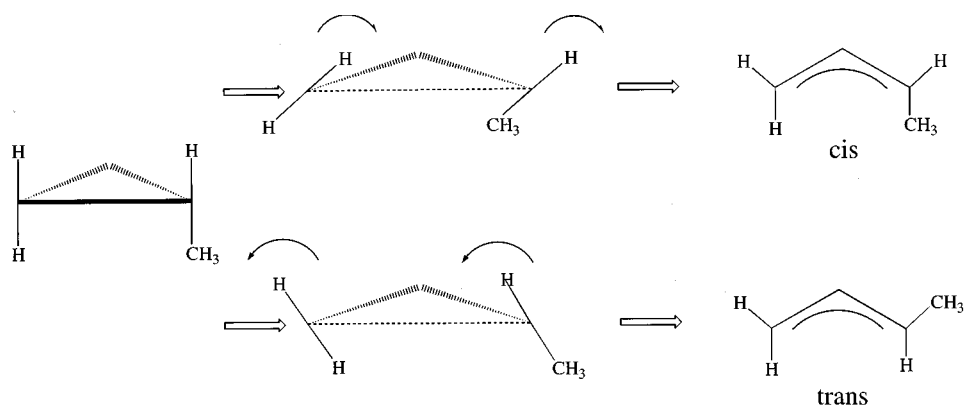


FIG. 11. Schematic representation of methylcyclopropylidene ring opening to triplet *cis/trans* 1,2-butadiene. Top: clockwise–clockwise; bottom: counterclockwise–counterclockwise.

cluded from further discussion because the reaction proceeds via the lowest energy pathway. In addition, the rigorous identification of methylpropargyl at collision energy of 45.0 kJ mol^{-1} explicitly rules out a [1,3]-H-shift to 1,3-butadiene, since the last would decompose to 1,3-butadienyl-1 or 1,3-butadienyl-2. Even at our lowest applied collision energy, the formation of 1,3-butadienyl-2 seems rather unlikely. First, only the lowest limit of our high energy $P(E_T)$ cutoff overlaps with the maximum error as expected from thermodynamical data. Further, an increase in collision energy by only 20 kJ mol^{-1} hardly explains the formation of only 1,3-butadienyl-2 at lower, but methylpropargyl radicals at higher collision energy. Therefore, we conclude the reaction most likely proceeds via 1,2-butadiene and a carbon-hydrogen bond cleavage to methylpropargylene. Since no symmetry element is conserved from the initial addition to the final fragmentation step, the reaction can proceed on the 3A surface.

If we compare these dynamics with those of the reaction $C(^3P_j) + C_2H_4$ to propargyl and atomic hydrogen,²⁶ we find that the additional modes of the CH_3 group in the triplet 1,2-butadiene intermediate enhance the lifetime of the decomposing complex as compared to triplet allene. This yields a symmetric center-of-mass angular distribution at 23.3 kJ mol^{-1} collision energy as the result of a decomposing 1,2-butadiene complex holding a lifetime equal or exceeding its rotational period. As the collision energy increases, the angular distribution changes to a more forward peaked one as a consequence of the reduced 1,2-butadiene lifetime. The alternative interpretation of a symmetric exit transition state contributing to a symmetric angular distribution can be ruled out, since the fragmenting 1,2-butadiene belongs to the C_1 point group, and no H atoms can be interconverted to depart with equal probability into the center-of-mass angles θ and $\pi - \theta$.

C. Rotation axis and lifetime of the 1,2-butadiene complex

In the following paragraph, we investigate the rotational motion of the *cis/trans* 1,2-butadiene complexes to discriminate between 1- and 3-methylpropargyl. Since the angular distribution is forward peaked at higher collision energy, this requires the attacking carbon atom and the leaving hydrogen to be located on opposite sites of the rotation axis. Therefore, *trans* 1,2-butadiene complexes excited to B- and C-like rotations decompose solely through C–H₁ rupture to 3-methylpropargylene. On the other hand, the *cis* isomer can fragment via C–H₂/H₃ (A-rotations) as well as C–H₂ rupture (C-rotations; C-axis perpendicular to the molecular plane) to 1-methylpropargyl, but via C–H₁ cleavage (B-rotations) to 3-methylpropargyl.

We reduce the feasible rotational axis further, if we estimate the lifetime of 1,2-butadiene in terms of the osculating complex model. Based on the intensity ratio of 6 ± 3 at the poles of the angular distribution, the lifetime is calculated to be approximately one third of a rotation period, i.e., 0.02 – 0.05 ps (A-axis), and 0.3 – 0.55 ps (B/C-axes), cf. Table III.

TABLE IV. Fractional energy release into the translational ($\langle E_T \rangle$), rotational, ($\langle E_{rot} \rangle$), and vibrational, ($\langle E_{vib} \rangle$) degrees of freedom calculated for $K=0$ at both collision energies.

	$E_{coll}=23.3 \text{ kJ mol}^{-1}$	$E_{coll}=45.0 \text{ kJ mol}^{-1}$
$\langle E_T \rangle$	31 ± 4	34 ± 3
$\langle E_{rot} \rangle$	15 ± 2	7 ± 1
$\langle E_{vib} \rangle$	57 ± 2	57 ± 2

Since reaction with collision times less than 0.1 ps follow direct dynamics,⁴⁶ $T(\theta)$ should be strongly forward peaked at the collision energy of 45.0 kJ mol^{-1} . Therefore, rotations around the A axis of *cis/trans* 1,2-butadiene can be clearly ruled out and only B- and/or C-like rotations account for the reactive scattering signal. Here, the almost in-plane C-like rotations give rise to extremely low K states of 1,2-butadiene. This in-plane rotation could be associated with preferentially low K values populated in the methylpropargyl product (Sec. V D).

D. Exit transition state and energy partitioning

Since both translational energy distributions $P(E_T)$ s peak at 15 – 60 kJ mol^{-1} , the C–H bond rupture in triplet 1,2-butadiene does not represent an ideal RRKM system with a loose transition state. Our data rather indicate a significant geometry change from the fragmenting complex to the methylpropargyl radicals as evident from carbon–carbon bond lengths reduced by 0.1 – 0.2 \AA . Further, the bond angle of the allene-subunit in 1,2-butadiene opens up by 50° – 55° to a linear C–C–C-chain. The order of magnitude of the exit barrier is consistent when compared to the reaction $C(^3P_j) + C_2H_4 \rightarrow 1-C_3H_3 + H$.²⁶ Here, the allene intermediate fragments to propargyl radicals and atomic hydrogen, and the barrier ranges between 28 and 43 kJ mol^{-1} .

In addition, we analyze the partition of total available energy into product rotation, vibration, and translation. This enables us to compare the collision energy dependent fractional energy release in the vibrational degrees of freedom. When these data are compared to the C/C₂H₄ system, the role of the propylene CH₃ group to boost the lifetime of the fragmenting complex is elucidated. Since both methylpropargyl radicals represent prolate asymmetric tops with asymmetry parameters $\kappa = -0.99$ and -0.81 , 3- and 1-methylpropargyl, respectively, their energy levels are approximated as those of an ideal, rigid symmetric top. Since our crossed beam experiments cannot resolve the rotational structure, no information on the K distribution can be supplied. Hence, we estimate the maximum vibrational energy release choosing $K=0$. Our calculation reveals an almost constant fraction of $57 \pm 2\%$ channeling into the vibration, cf. Table IV. The reaction $C(^3P_j) + C_2H_4 \rightarrow 1-C_3H_3 + H$ ²⁶ however, shows a decreasing fraction of vibrational energy release from 50% to 43% in the triplet allene intermediate as the collision energy rises. These patterns clearly indicate an enhanced partition of the total available energy into vibration as the vibrational degrees of freedom rise from 15 (decomposing allene complex, C₃H₄) to 24 (fragmenting 1,2-butadiene, C₄H₆).

VI. CONCLUSIONS

The reaction between ground state carbon atoms, $C(^3P_j)$, and propylene, $C_3H_6(X^1A')$, was studied at average collision energies of 23.3 and 45.0 kJ mol^{-1} using the crossed molecular beam technique. This reaction proceeds on the 3A surface via an addition of the carbon atom to the π -orbital to form triplet methylcyclopropylidene, followed by ring opening to *cis/trans*-1,2-butadiene. Within 0.3–0.6 ps, this complex decomposes via carbon–hydrogen bond rupture to atomic hydrogen and methylpropargyl radicals. Compared to the $C(^3P_j)/C_2H_4$ system studied recently in our group,²⁶ the methyl group enhances the lifetime of the decomposing intermediate and reduces the cone of acceptance of the approaching carbon atom to propylene. This effects the approach geometries significantly and closes the strongly forward-scattered microchannel to high K -states excited propargyl isomer, *l*- C_3H_3 , as found in Ref. 26. Finally, the CH_3 group breaks the symmetry of the reaction surface to 3A vs $^3A''$ as found in the $C(^3P_j)/C_2H_4$ system. The explicit identification of C_4H_5 under single collision conditions represents an additional example of a carbon–hydrogen exchange in reactions of ground state carbon with unsaturated hydrocarbons. This versatile concept represents an alternative pathway to form hydrocarbon radicals in combustion processes, chemical vapor deposition, and the interstellar medium.

Further investigations of this reaction should focus on the hitherto unresolved isomer assignment, i.e., 1- versus 3-methylpropargyl. If the adiabatic ionization potentials differ by more than 0.5 eV, this system resembles an ideal candidate to be investigated via VUV photon induced ionization on the chemical dynamics beamline at the advanced light source (ALS). Further, photolysis of the reaction products at 193 nm in the interaction region yields $H+C_4H_4$ or $C_2H+C_2H_4$ (1-methylpropargyl), but $CH_3+C_3H_2$ and $C_3H_3+CH_2$ in the case of 3-methylpropargyl. Finally, partially deuterated propylene represents an excellent option if the 1,2-3-deutero-butadiene complex fragments via C–D bond rupture, we will detect 1-methylpropargyl at $m/e=53$; H atom loss, however, gives rise to $m/e=54$ pattern. The mission continues.

Note added in proof. Prior to acceptance of this manuscript, we performed a crossed beam reaction of $C(^3P_j)$ with the second C_3H_6 isomer, cyclopropylene. However, no reactive scattering signal could be probed, and the reaction cross section is at least 50 times lower as compared to the title reaction.

ACKNOWLEDGMENTS

R.I.K. is indebted the Deutsche Forschungsgemeinschaft for a post-doctoral fellowship. We thank the electronics shop, Department of Chemistry, UC Berkeley, for designing the new resistance triggered polarity switchbox of our carbon source. This work was supported by the Director, Office of Energy Research, Office of Basic Energy Sciences, Chemical Sciences Division of the U.S. Department of Energy under Contract No. De-AC03-76SF00098.

- ¹P. R. Westmoreland, A. M. Dean, J. B. Howard, and J. P. Longwell, *J. Phys. Chem.* **93**, 8171 (1989).
- ²J. A. Millar and C. F. Melius, *Comb. Flame* **91**, 21 (1992).
- ³H. Wang and M. Frenklach, *J. Phys. Chem.* **98**, 11 465 (1994).
- ⁴M. A. Weissman and S. W. Benson, *J. Phys. Chem.* **92**, 4080 (1988).
- ⁵W. C. Hung, M. L. Huang, Y. C. Lee, and Y. P. Lee, *J. Chem. Phys.* **103**, 9941 (1995).
- ⁶E. Herbst, *Angew. Chem.* **102**, 627 (1990).
- ⁷Symposium on Titan, ESA, ESA Special Publication 338 (ESTEC, Noordwijk, 1992).
- ⁸J. I. Lunne, *Chemical Eng. News* **1995**, 52.
- ⁹D. Toublanc, J. P. Parisot, J. Brillet, D. Gautier, F. Raulin, and C. P. McKay, *Icarus* **113**, 2 (1995).
- ¹⁰K. H. Baines, M. E. Mickelson, L. E. Larson, and D. W. Ferguson, *Icarus* **114**, 328 (1995).
- ¹¹R. I. Kaiser and K. Roessler, *Astrophys. J.* **475**, 144 (1997).
- ¹²A. M. Mansour, H. A. Elkhalk, and K. Roessler, Report Jul-3002 (1994).
- ¹³K. Ohta, M. Shiotani, J. Sohma, and A. Hasegawa, M. C. R. Symons, *Chem. Phys. Lett.* **136**, 465 (1987).
- ¹⁴T. T. Nguyen and K. D. King, *J. Phys. Chem.* **85**, 3130 (1981).
- ¹⁵T. T. Nguyen and K. D. King, *Int. J. Chem. Kin.* **14**, 613 (1982).
- ¹⁶R. D. Kern, H. J. Singh, and C. H. Wu, *Int. J. Chem. Kin.* **20**, 731 (1988).
- ¹⁷R. P. Duran, V. Amorebieta, and A. J. Colussi, *J. Phys. Chem.* **92**, 636 (1988).
- ¹⁸P. K. Chou and S. R. Kass, *J. Am. Chem. Soc.* **113**, 697 (1991).
- ¹⁹P. J. Krusic, J. P. Jesson, and J. K. Kochi, *J. Am. Chem. Soc.* **91**, 4566 (1969).
- ²⁰C. Roberts and J. C. Watson, *J. Chem. Soc. Perkin. Trans.* 879 (1983).
- ²¹F. W. King and H. Schlegel, *J. Magn. Res.* **22**, 389 (1976).
- ²²T. T. Nguyen and K. D. King, *Int. J. Chem. Kin.* **14**, 613 (1982).
- ²³T. T. Nguyen and K. D. King, *J. Phys. Chem.* **85**, 3130 (1981).
- ²⁴S. Olivena and A. Scole, *J. Am. Chem. Soc.* **113**, 87 (1991).
- ²⁵H. Chen, B. F. G. Johnson, J. Lewis, D. Braga, and F. Grepioni, *J. Organometallic Chem.* **398**, 159 (1990).
- ²⁶R. I. Kaiser, Y. T. Lee, and A. G. Suits, *J. Chem. Phys.* **105**, 8705 (1996).
- ²⁷R. I. Kaiser, D. Stranges, Y. T. Lee, and A. G. Suits, *J. Chem. Phys.* **105**, 8721 (1996).
- ²⁸R. I. Kaiser, Y. T. Lee, and A. G. Suits, *J. Chem. Phys.* **103**, 10 395 (1995).
- ²⁹R. I. Kaiser, C. O. Ochsenfeld, M. Head-Gordon, Y. T. Lee, and A. G. Suits, *Science* **274**, 1508 (1996).
- ³⁰C. Ochsenfeld, R. I. Kaiser, Y. T. Lee, A. G. Suits, and M. Head-Gordon, *J. Chem. Phys.* (to be published).
- ³¹Y. T. Lee, J. D. McDonald, P. R. LeBreton, and D. R. Herschbach, *Rev. Sci. Instrum.* **40**, 1402 (1969).
- ³²R. I. Kaiser and A. G. Suits, *Rev. Sci. Instrum.* **66**, 5405 (1995).
- ³³G. O. Brink, *Rev. Sci. Instrum.* **37**, 857 (1966).
- ³⁴N. R. Daly, *Rev. Sci. Instrum.* **31**, 264 (1960).
- ³⁵M. S. Weis, Ph.D. thesis, University of California, Berkeley (1986).
- ³⁶M. Vernon, LBL-Report 12 422 (1981).
- ³⁷R. I. Kaiser, D. Stranges, Y. T. Lee, and A. G. Suits (unpublished).
- ³⁸W. B. Miller, S. A. Safron, and D. R. Herschbach, *Discuss Faraday. Soc.* **44** **108**, 291 (1967).
- ³⁹W. B. Miller, Ph.D. thesis, Harvard University, Cambridge (1969).
- ⁴⁰J. O. Hirschfelder, C. F. Curtiss, and R. B. Bird, *Molecular Theory of Gases and Liquids* (Wiley, New York, 1954).
- ⁴¹*Handbook of Chemistry and Physics* (CRC Press, Boca Raton, 1995).
- ⁴²N. J. Turro, *Modern Molecular Photochemistry* (University Science Books, Milla Valley, 1991).
- ⁴³R. I. Kaiser, Y. T. Lee, and A. G. Suits (unpublished).
- ⁴⁴See discussion in Ref. 26.
- ⁴⁵S. S. Shaik and E. Canadell, *J. Am. Chem. Soc.* **112**, 1446 (1990).
- ⁴⁶R. D. Levine, and R. B. Bernstein, *Molecular Reaction Dynamics and Chemical Reactivity* (Oxford University Press, Oxford, 1987).